COASTAL INCENTIVE GRANT (CIG) PROGRAM

GEORGIA COASTAL MANAGEMENT PROGRAM

Project Title	**Quantification of the energy potential from tidal streams for Rose Dhu Island, Georgia**
Grantee	Georgia Tech
Principal Investigator Name	Francesco Fedele, Thorsten Stoesser and Kevin Haas
PI Address	210 Technology Circle Savannah Georgia 31407
PI Phone Number	9129666785
Grant Manager Name and phone number if different from PI	
Reporting Period	
	■ Final Report ☐ Status Report
Date of Report	April 07 2012

Summary of activities: Objective 1 has been fulfilled. In particular, we have completed Tasks 1 and 2 undertaking studies via experiments and flow measurements that helped identifying the hotspot for high tidal stream energy potential. Indeed, one hotspot for tidal currents was determined to be on the west side of Rose Dhu Island. We have also assessed the Hydrodynamics of the channels adjacent to Rose Dhu Island and explain why the 'hot spot' exists.

Task 3 has been completed and Objectives 2 and 3 are fulfilled. In particular, we have applied computational fluid dynamics (CFD) to quantify in great details the current flow dynamics. Simulations with a finer numerical grid have been performed for an improvement in the accuracy of our results. In the simulation, the friction factor in wetlands is selected to be ten times higher than in the main channel. This value was chosen based on similar studies in the literature. Using the vegetation count from field measurements, the actual friction factor is computed using drag resistance formulas and incorporated into the model. Tidal energy assessment has been conducted and an estimate of the total power that can be extracted is provided.

Finally, as regard to Objective 4 the first of the two technical seminars has been organized and held at Rose Dhu last August 20 to disseminate project results and findings. The second seminar is planned at Tybee Island in April-May 2012.

Task Objectives Completed:

Objective 1: Identification of the hot spots for high tidal stream energy potential via experiments and flow measurements; hydrodynamics of the channels adjacent to Rose Dhu.

1. **Problems encountered and unanticipated delays:** none

2. **Status:** completed

3. **Deliverables:** Data collection of current and bathymetry measurements.

Task #1. Short term boat based measurements.

To find and characterize the hotspots for tidal currents, velocity measurements from a boat equipped with an Acoustic Doppler Velocity Profiler (ADCP) was carried out around Rose Dhu Island on October 19 and 20, 2010. As shown in the left panel of Figure 1, the area of interest was divided between the west and east side of Rose Dhu Island. On October 19, the current measurements were made on the east side of the island, covering both a flood and ebb tide. As shown in the right panel of Figure 1, the currents were fairly weak, with peak magnitudes between 50 and 60 cm/s. On October 20, the measurements were completed on the west side of the island where the current peaked closer to 100 cm/s. Therefore, the hotspot for tidal currents was determined to be on the west side of the island as shown by the black circle in Figure 1.

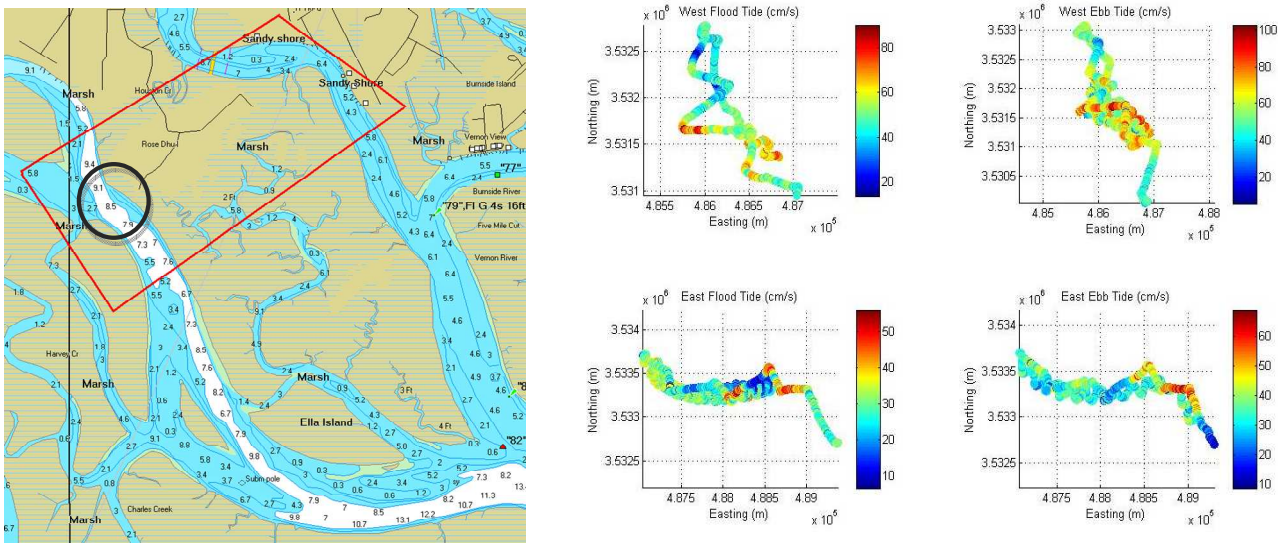

Figure 1: Left: *Bathymetric map of Rose Dhu Island. The red box outlines the area of interest on the east and west side of the island. From boat based velocity measurements a hotspot of high kinetic energy has been identified on the west side (black circle).* ***Right:*** *Plots of the velocity magnitude measurements on the west and east side of the island over a flood and ebb tide.*

Task #2. Detailed bathymetric and vegetation measurements.

In order to facilitate detailed numerical modeling of the tidal current hotspot, high resolution bathymetric data was collected. Surveying was completed using a 16 ft Zodiac outfitted with kinematic GPS synchronized with a single beam fathometer. The bathymetric survey was completed on November 22 and 29, 2010. This survey resulted in over 235,000 soundings of the full area of interest to be modeled including both the upstream branches and a relatively large creek feeding into the domain. As can be seen in Figure 2, the main channel along the side of Rose Dhu Island where the hotspot is located has depths ranging from 8-11 m.

On December 20 and 21, 2010 a vegetation count was performed in the marsh near the tidal current hotspot on the west side of Rose Dhu Island. Twenty-five different sites were measured covering a variety of vegetation densities. A 1x1m patch was marked and the vegetation within the four quadrants were counted and measured. An example photo from one such site is shown in Figure 3 below.

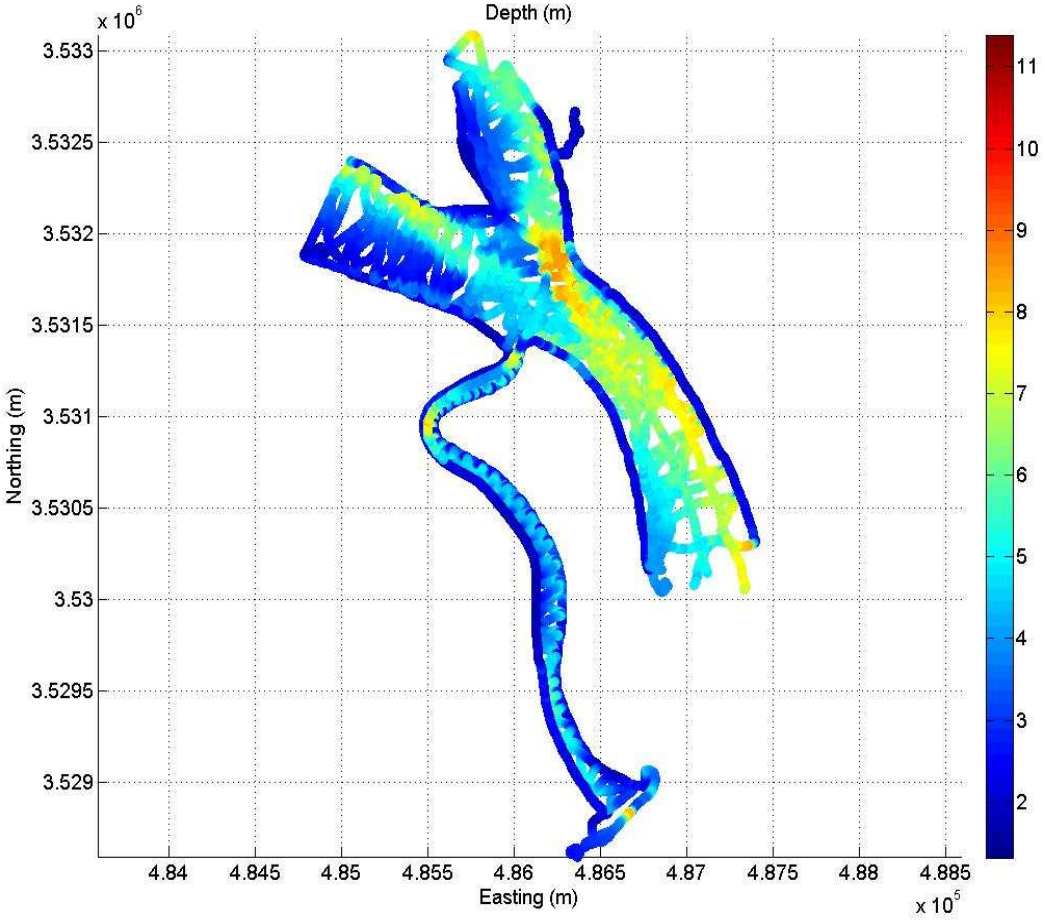

Figure 2*: Map of the bathymetric soundings from the west side of Rose Dhu Island.*

Figure 3*: Example photo of vegetation on the west side of Rose Dhu Island near the tidal current hotspot. The red string maps out the 1x1m box where the vegetation was counted.*

Field measurements used to previously identify hot spots for high tidal stream energy potential were further analyzed to characterize the hydrodynamics of the channels adjacent to Rose Dhu Island. ADCP (Acoustic Doppler Velocity Profiler) measurements, taken October 20, 2010 on the west side of the island were chosen to be further studied due to their relatively high current magnitudes relative to those found on the east side. For every measurement location, the ADCP measured the east and north components of the current velocity along the water column at that point. The ADCP "bin averages" these measurements for every 0.5m below the water surface. In previous analyses, these measurements were averaged along the entire depth to identify potential tidal energy hotspots relative to the island in two-dimensional geographical space, Easting and Northing. Here, the ADCP measurements will be considered in three-dimensions, Easting, Northing, and depth as seen in Figure 4.

First, it was chosen to study solely the measurements that were part of complete transects of the channel as seen in Figure 5. This was done to (a) directly compare ebb and flood measurements, which follow the same tracks along these transects; (b) potentially perform channel flux calculations; (c) fully understand the hydrodynamics of the entire channel length. Each transect was then isolated and studied, comparing measurements from flood and ebb tide as shown in Figure 6.

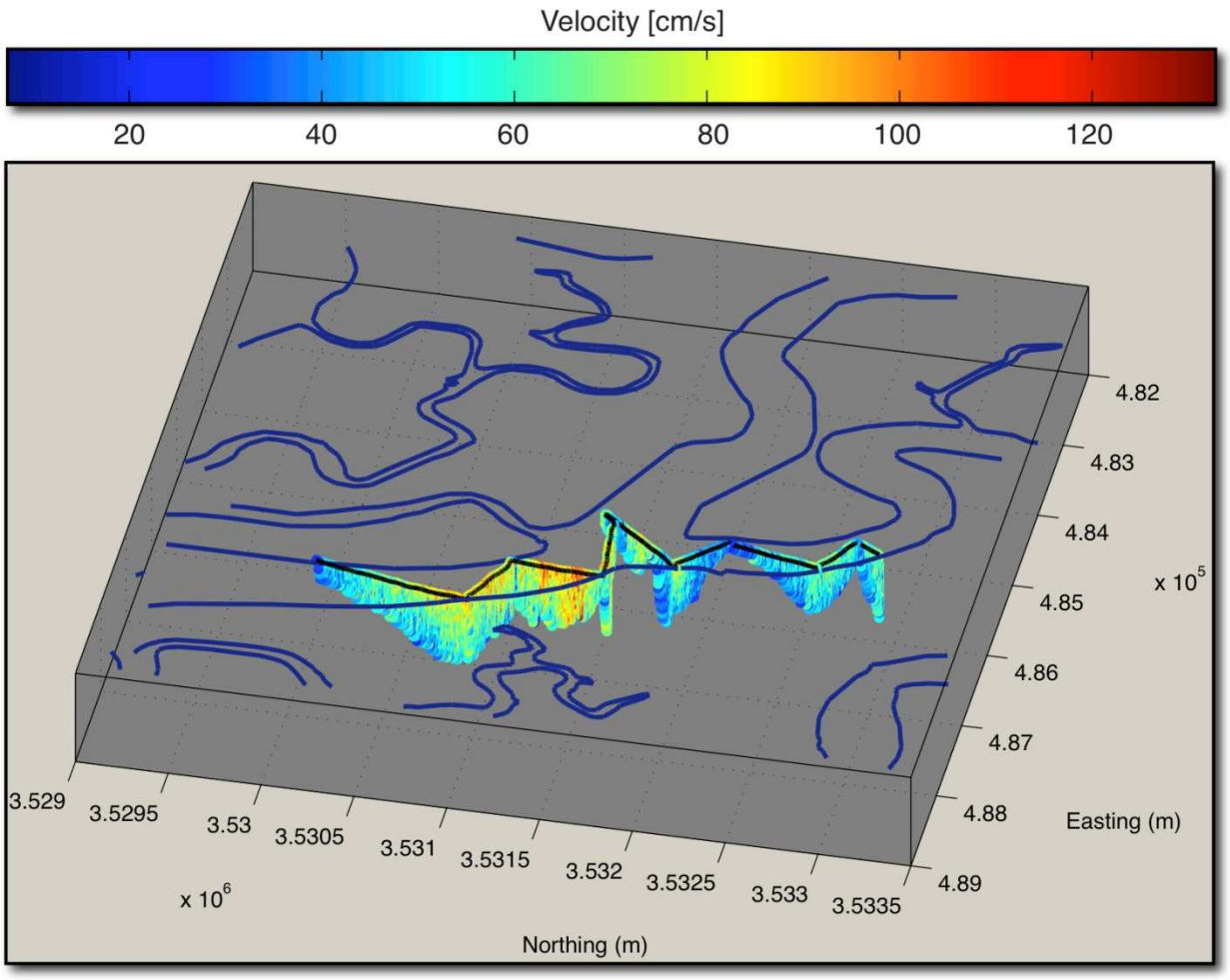

Figure 4: *Three-dimensional mapping of ADCP velocity measurements taken from October 20, ebb tide. Color mapping represents current velocity magnitudes in cm/s. Third dimension, vertical, represents depth. Black line represents boat track as plotted along a two dimensional plane at depth=0.*

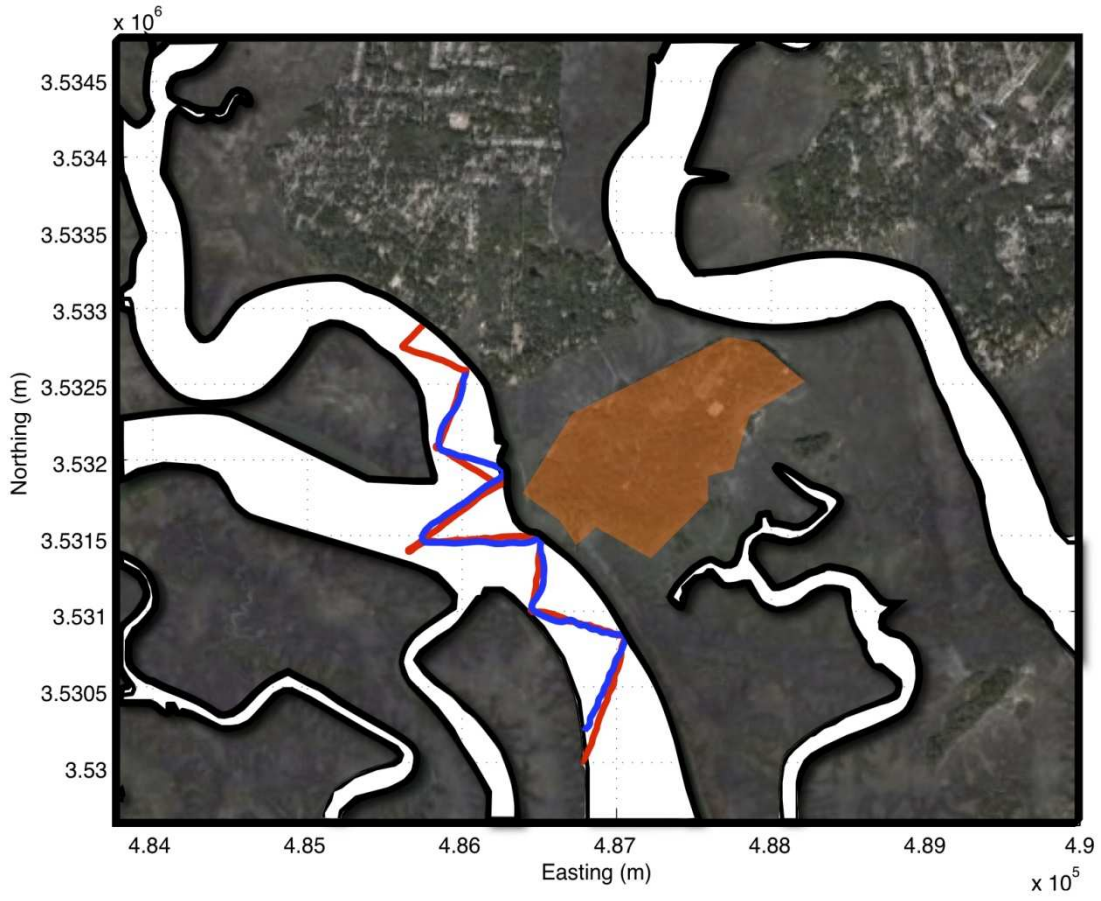

Figure 5: *Transects utilized for channel flow analysis. Channels are highlighted in white. Red line represents boat track (i.e. measurement locations) for October 20, ebb tide. Blue line represents boat track for October 20, flood tide. Orange shaded area represents Rose Dhu Island. Satellite imagery courtesy of Google Earth.*

As seen in Figure 6, for each transect across the channel the velocity measurements were plotted in two dimensions: velocity as a function of depth and distance across the channel. The contour profiles were plotted so as to be read from left to right and to match with the orientation of the transect in the map.

The velocity measurements originally were in north and east components. A rotation of the coordinate system for each point was performed in order to obtain components in the direction across the channel cross section and perpendicular to the cross section, referred to as cross and axial velocities respectively. After the coordinate transformation was complete the magnitude of the velocities were then taken and are shown in Figure 6. Then, the depth averaged axial and cross velocities were removed from the axial and cross velocities for a point in space (i.e. the mean was removed). Thus, what is left is the residual flow. Both cross and axial residuals are also shown in Figure 6. Doing this, we can more clearly see

velocity variations as a function of depth and distance across the channel as well as cross channel circulation.

In relation to tidal energy applications, this analysis can help identify the physical reasons why such 'hot spots' occur in addition to describing depth variation and cross channel circulation in current velocities as well as differences between ebb and flood tidal flow, potentially informative for tidal turbine installation considerations.

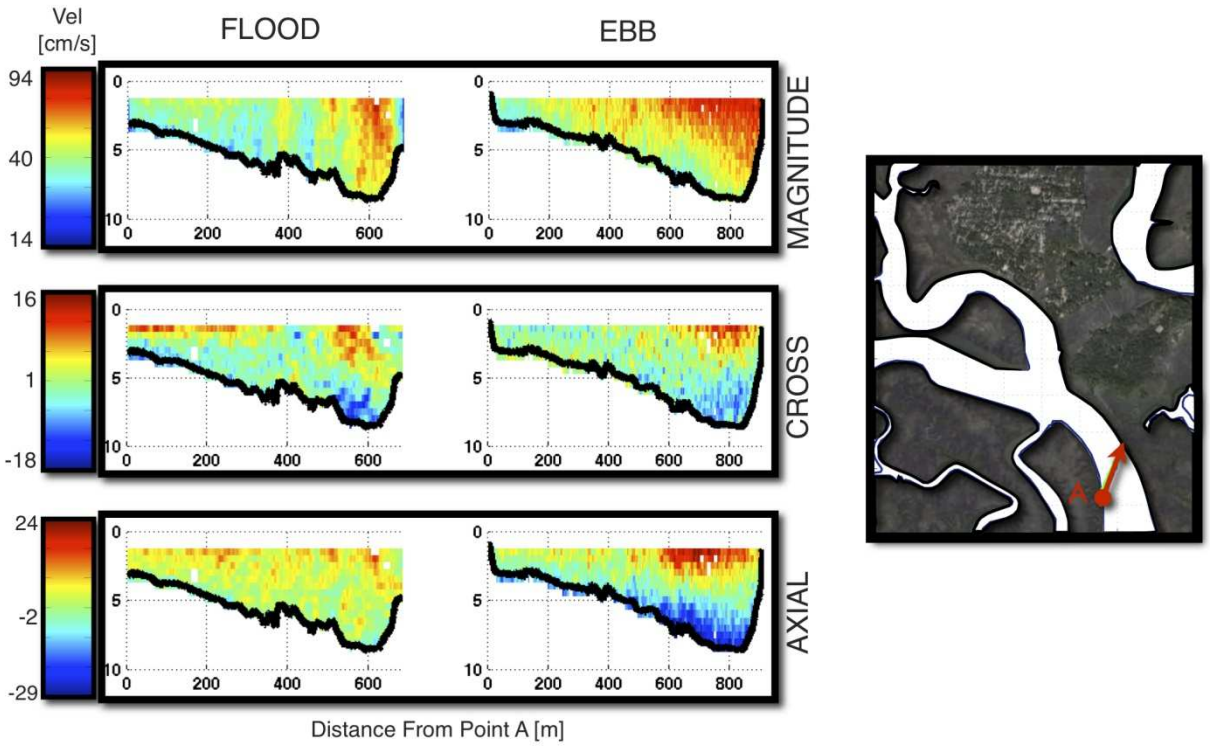

Figure 6: ***Left:*** *Example velocity profile of transect, pictured right. Columns represent data obtained from October 20, flood tide (left) and October 20, ebb tide (right). First Row from top represents velocity magnitudes. Second row represents cross channel flow, depth-averaged mean flow removed. Positive values represent flow traveling away from point A, negative values represent flow traveling towards point A. Third Row represents axial flow, depth –averaged mean flow removed. Positive values represent areas of flow faster than the mean flow in the respected ebb/flood direction and negative values represent areas of slower flow. All images 'smoothed' using a moving average to highlight spatial structures of current velocity. Satellite imagery courtesy of Google Earth.*

In response to the findings from the analysis exemplified in Figure 6, another field campaign was performed on November 27 and December 22, 2011 to gain further insight into the hydrodynamic differences between the ebb and flood tidal flows surrounding Rose Dhu. Boat based ADCP measurements, as in the previous field campaign, were taken along predetermined transects multiple times. The transects, as pictured in Figure 7, were positioned to observe the most dynamic and energetic areas of the channel concluded from the previous campaign and were oriented perpendicular to the curvatures of the channels to facilitate the decomposition of current velocities into cross channel and axial components. However most importantly, in this campaign, fewer transects were charted over a smaller spatial domain, allowing for individual transects to be measured many more times at a higher temporal frequency throughout the tidal cycle to better resolve the temporal evolution of the channel.

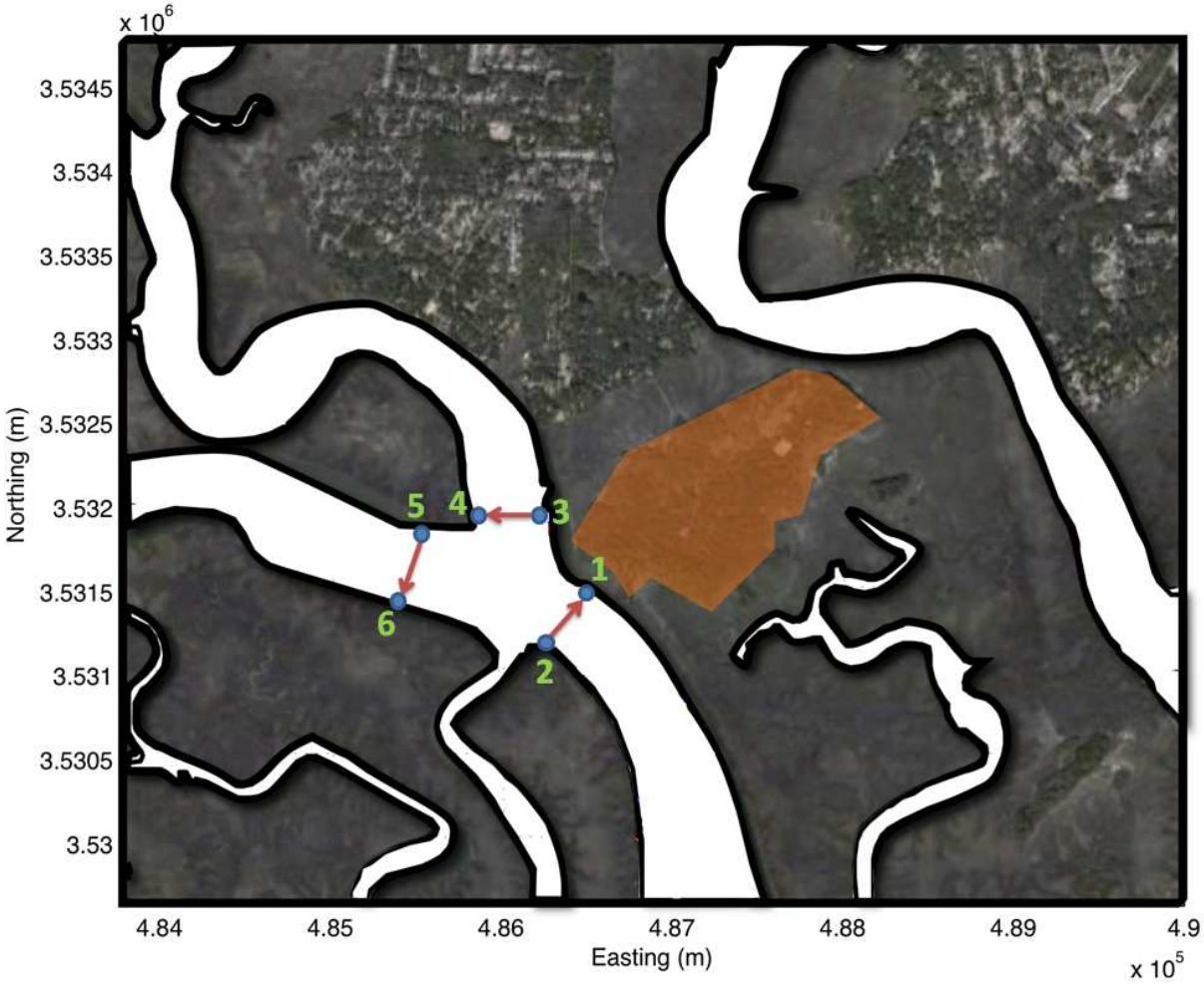

Figure 7: *Charted transects for field campaigns carried out on November 27 and December 22, 2011. Arrows indicate the consistent direction of transversal for each of the transects: 2-1, 3-4, and 5-6. Orange shaded area represents Rose Dhu Island. Satellite imagery courtesy of Google Earth.*

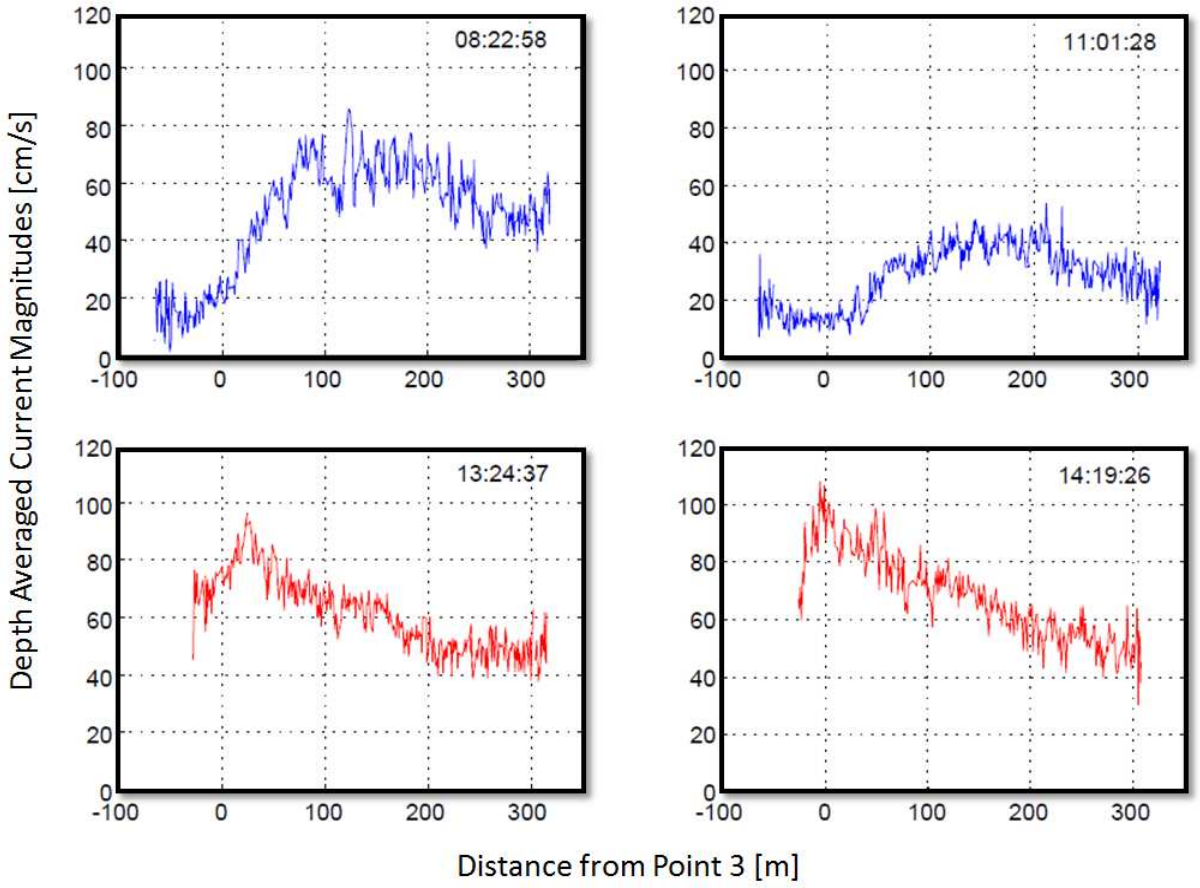

Figure 8: *Depth averaged current magnitudes from transect 3-4 for measurements taken on November 27, 2011 at various times of the day. Blue and red lines represent measurements taken during flood and ebb tide respectively. Timestamp of measurement located in upper right hand corner of each panel.*

Figure 8 highlights both the spatial and temporal progressions of tidal current magnitudes as measured along transect 3-4. As expected, as the tidal cycle progresses throughout the day, the tidal current magnitude across the overall channel wanes and rises. More intriguing however, is the migration of localized areas of maximum and minimum tidal currents, or 'hot spots,' across the channel between flood and ebb tide, further emphasized in Figure 9.

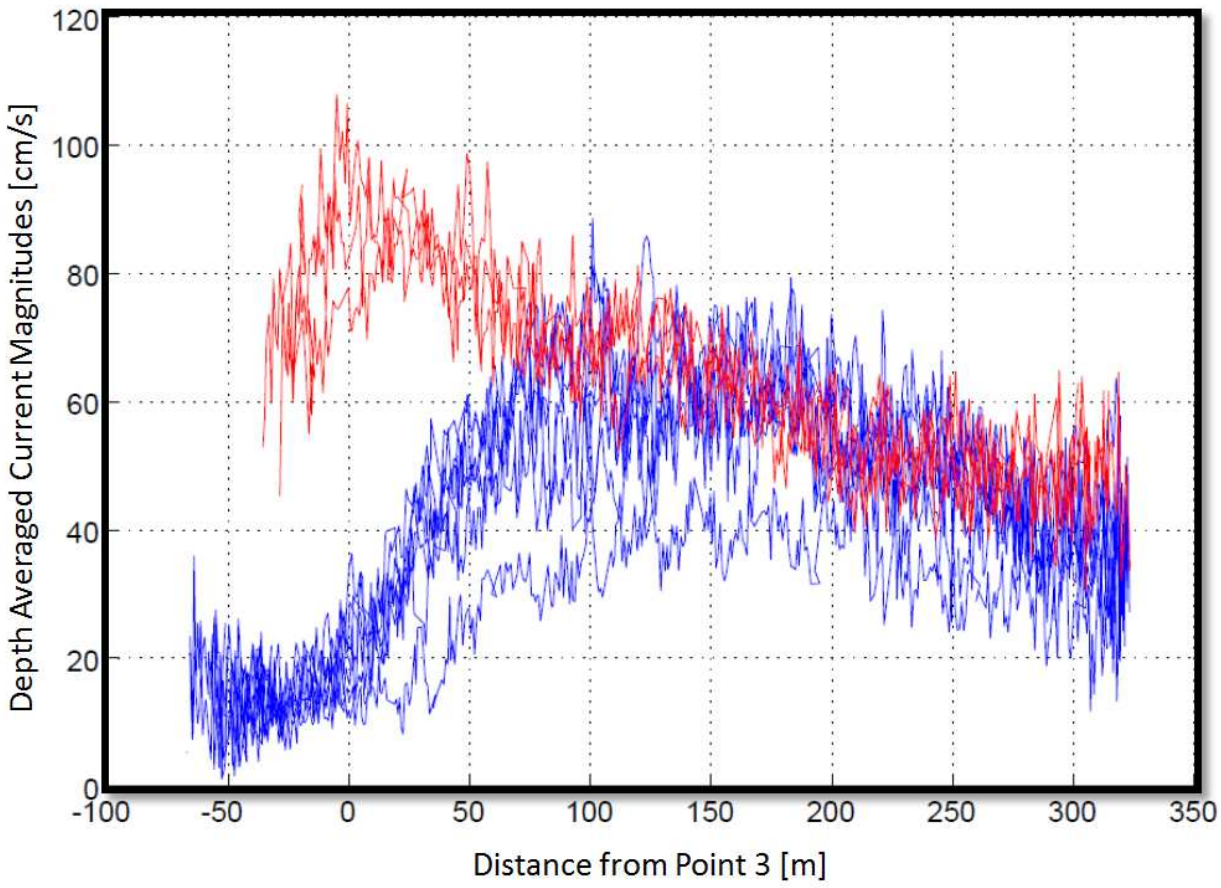

Figure 9: *Superimposed depth averaged current magnitudes for transect 3-4 from all measurements taken on November 27, 2011. Blue and red lines represent measurements taken during flood and ebb tide respectively.*

The analysis was further expanded by the two dimensional representation of the channel currents. An example of this, for transect 2-1, is shown in Figure 10. Similar to the depth averaged values shown in Figure 8, the magnitudes strengthen and diminish as the tidal cycle progresses. Again, pockets of high current velocities are present and migrate with the tidal cycle. With this two dimensional analysis however, one can observe the depth variation and extent of the 'hot spots' within the water column as a function of the tidal stage.

For tidal energy applications, this movement of tidal energy 'hot spots' is relevant for the selection of the assembly location. An optimized, fixed installation would not only need to capture a 'hot spot' but also encompass it for an extended period of time in the tidal cycle; thus a moving, dynamic 'hot spot' between tidal stages complicates the selection process.

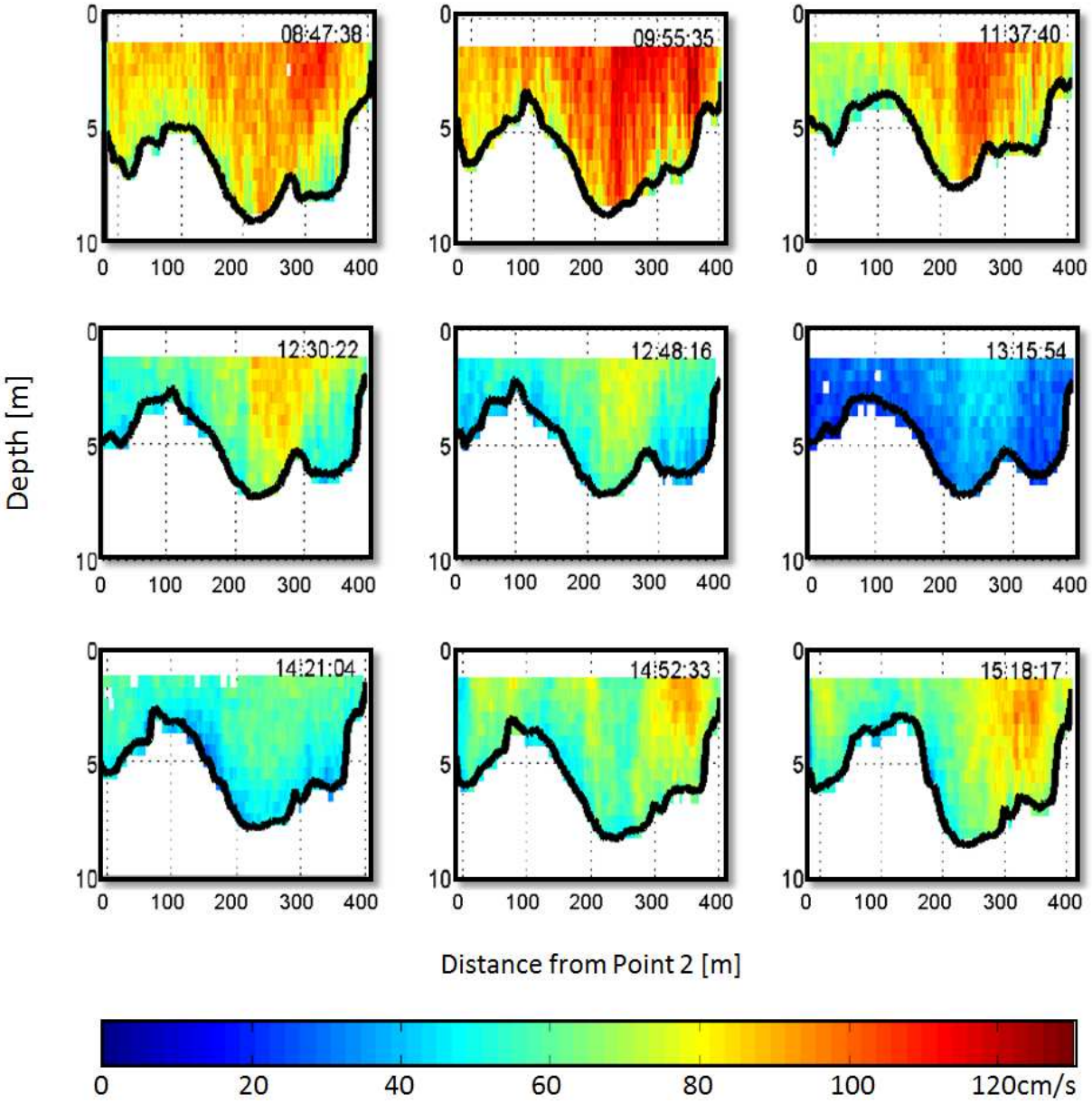

Figure 10: *Example velocity profiles of current magnitudes for transect 2-1 from measurements taken on December 22 2011. Timestamp of measurement located in upper right hand corner of each panel.*

Objective 2: quantify in great details current flow dynamics, turbulence structures and their statistics via computational fluid dynamics simulations.

1. **Problems encountered and unanticipated delays:** none

2. **Status:** completed.

3. **Deliverables:** results of current flow dynamics around the identified hot spot of high tidal energy potential via CFD simulations; comparisons of simulations with measurements.

Task #3. Computational Fluid Dynamics (CFD) Modeling.

Numerical Model

In this study, the finite volume coastal ocean model (FVCOM) is employed to simulate the tidal flow in and out of the Ogeechee estuary. FVCOM is a three-dimensional, free-surface primitive equations model originally developed by Chen et al. (2003). The model uses unstructured triangular grids in the horizontal and σ-coordinate transformation in the vertical for a better representation of the irregular bottom topography. The governing equations of the model are the momentum and continuity equations which are closed using the Mellor and Yamada level 2.5 turbulence closure scheme (Mellor and Yamada 1982) for vertical mixing and the Smagorinsky turbulence closure scheme (Smagorinsky 1963) for horizontal mixing. These governing equations are solved in the integral form by computing fluxes between non-overlapping horizontal triangular control volumes. This finite-volume approach used in FVCOM combines the best of finite-element methods for geometric flexibility and finite-difference methods for simple discrete structures and computational efficiency (Chen et al. 2006). FVCOM also includes a wet/dry point treatment method for simulating the flooding and drying processes observed during the high and low tides. A detailed description of the model and its capabilities can be found in Chen et al. (2006).

Computational domain and boundary conditions

Computational domain of the present simulation covers the entire Ogeechee estuary including the main channel and the inter-tidal marsh zones (also referred to as the wetlands). This is shown in Fig. 11 where the horizontal numerical grid along with a satellite image of the estuary on the background is presented. The numerical grid at the open boundary located in the ocean is coarse with a spacing of ~300m. However at regions close to the Rose Dhu Island, a relatively fine grid is employed with a spacing of ~50m. The mean water depth at each of these numerical grid points is calculated through an interpolation of available bathymetric data consisting of field measurements close to the Rose Dhu Island, survey data from the National Oceanic and Atmospheric Administration (NOAA) database and the National Wetlands Inventory. Figure 12 shows the contours of mean water depth obtained after interpolation of the bathymetric data. The observed variability in water depth indicates heterogeneity in

channel characteristics (like the sinuosity or presence of small barrier islands) that can possibly lead to a local acceleration/deceleration of the flow. Therefore, a 3-D numerical simulation (with a terrain-following grid) like in the present study can be useful in capturing such flow features along with a good estimation of tidal elevation and current magnitudes.
The model is driven by 6 major tidal constituents (S2, M2, N2, K2, K1, and O1) specified at the open boundary, the amplitude and phase of which are computed from ADCIRC tidal database (http://www.unc.edu/ims/ccats/tides/tides.htm). The water levels and current magnitudes within the domain are zero initially and tidal forcing at the open boundary is ramped up to its actual value over two days to avoid any numerical instability. In total, the model is run over a 32 day period (including the ramping) such that both spring and neap tides within a lunar month are simulated. Since the field measurements are carried out during a spring tide, the model predictions corresponding to a spring tide are identified and compared with the field data.

Results and Discussion

Numerical model validation

Figure 13 shows a comparison of simulated water levels (represented by red line) with field measurements (plotted as black symbols). Water levels predicted by the model show peak values varying from -1.1m observed during the ebb tide to +1.1m observed during the flood tide. Due to the lack of field measurements over the entire tidal cycle, peak values of water levels are not very clear from the measurements. Therefore, a better validation of the simulated water levels is performed using the observed tidal elevations obtained from the NOAA's Coffee Bluff Station. This is shown in Figure 14 where the time-series for the entire month of October is plotted. The simulated water levels seem to be in perfect agreement with the measurements suggesting that the model is highly successful in capturing the tidal dynamics in the Ogeechee estuary.

For an understanding of the flooding and drying process in the estuary, contours of the depth-averaged current magnitude are visualized in Figs. 15 and 16 at a selected time-instance when the water enters and leaves the estuary, i.e. during the flood and ebb tides respectively. It is obvious that the current magnitudes in general are quite low close to the ocean because of the presence of higher water depths. Higher current magnitudes due to local flow acceleration can be observed at locations where channel constrictions or shallow water depths are encountered. A comparison of Figs. 15 and 16 indicate that the ebb tide currents are much stronger than the flood tide currents suggesting tidal asymmetry in the Ogeechee estuary. This dominance of ebb tides over food tides can be observed clearly in Figs. 17 and 18 where zoomed in plots of the currents are presented for regions close to the Rose Dhu Island. Huang et al. (2008) in their numerical studies of tidal flow in Okatee Creek, SC also reported this behavior and suggested that the storage volume provided by intertidal zones/wetlands play a significant role in the production of tidal asymmetry. During a flood tide when water enters the estuary, excess water in the main channel flushes out filling up the intertidal zones. Similarly during an ebb tide when water flows out of the estuary, water from the intertidal zones flows back into the main channel. The current vectors shown in Figs. 17 and 18 clearly depict this flooding and drying process revealing the importance of intertidal zones in providing additional storage for water.
Figure 19 shows the time series of simulated current magnitudes at a chosen location close to the Rose Dhu Island. The current magnitudes as expected are higher during the spring tides with values reaching a maximum of 1.0 m/s. Similarly the magnitudes are low during the neap tides with values reaching up

to 0.5m/s. An overall comparison also shows that the current magnitudes in general correspond to the tidal elevations (Fig. 14) with a small phase difference.

A quantitative comparison of the tidal current magnitude as obtained from simulations against the ADCP field measurements is performed in Figure 20. Few locations close to the Rose Dhu Island are chosen and current magnitudes are compared for both the flood and ebb tides. A perfect match between measured and computed data should result in the points falling close to the 45 degree line (in black). However, most of the points fall in between the dashed lines representing a 25% error margin between measured and computed data. A thorough analysis has been performed through several numerical simulations to investigate the reason behind this under-prediction of current magnitudes. Findings from the investigation of three parameters namely: (a) numerical grid resolution, (b) bottom friction including the vegetative roughness in the flood plains, and (c) bathymetry are presented below.

(a) Numerical grid resolution

It is often believed that the finer the numerical grid, better the accuracy of the simulation due to reduced numerical errors. However, in this study it was observed that a local grid refinement close to the Rose Dhu Island did not improve the accuracy of the results. Better results were observed only after the grid refinement at locations downstream of the Rose Dhu Island indicating that it is of utmost importance to completely resolve the smaller creeks branching out from the main tidal channel. This allows for the larger inflow of water into the channels, meaning higher current magnitudes. Further simulations needs to be carried out to identify these types of locations where it is necessary to have finer grid resolution.

(b) Bottom friction and vegetative roughness

Influence of bottom friction factors and vegetative roughness (in the wetlands) on the current magnitudes has been investigated through several numerical simulations. In general, the magnitudes were not influenced by these parameters and showed no improvement in the accuracy. It is believed that there are more important factors influencing the current speeds than the friction in the tidal channels.

(c) Bathymetry

Although reliable bathymetry data was available from the recent field surveys close to the Rose Dhu Island, data elsewhere (obtained from NOAA) is believed to be not up to date. This is because most of the NOAA surveys were conducted a few decades back and the bathymetry would have changed significantly since then due to the erosion and deposition of sediment in these tidal channels. It was observed through several numerical simulations that the current magnitudes are highly influenced by the bathymetry or the water depth in the tidal channels. For instance, in one of the simulations an increase in water depths by 50cms at a few locations downstream of Rose Dhu had resulted in a 20% increase in current speeds. Therefore it is imperative that the bathymetry data used in the simulation is right. Another potential source of error in bathymetry arises from the interpolation operation and smoothing performed (using the NOAA data points) to obtain the bathymetry at the numerical grid points. Smoothing of bathymetry data although introduces errors, cannot be avoided because it provides for numerical stability of the simulation. Presently efforts are being put into obtaining the right bathymetry at the grid points so that the current magnitudes are accurately predicted.

From Figures 13, 14 and 20 it is clear that the numerical model performed a good job in accurately simulating the tidal flow in the Ogeechee estuary. Therefore the velocity and water level elevation time-series data is recorded from the simulation (for the month of Oct 2010) and is used to estimate the annual power and future surface heights as discussed in the following section.

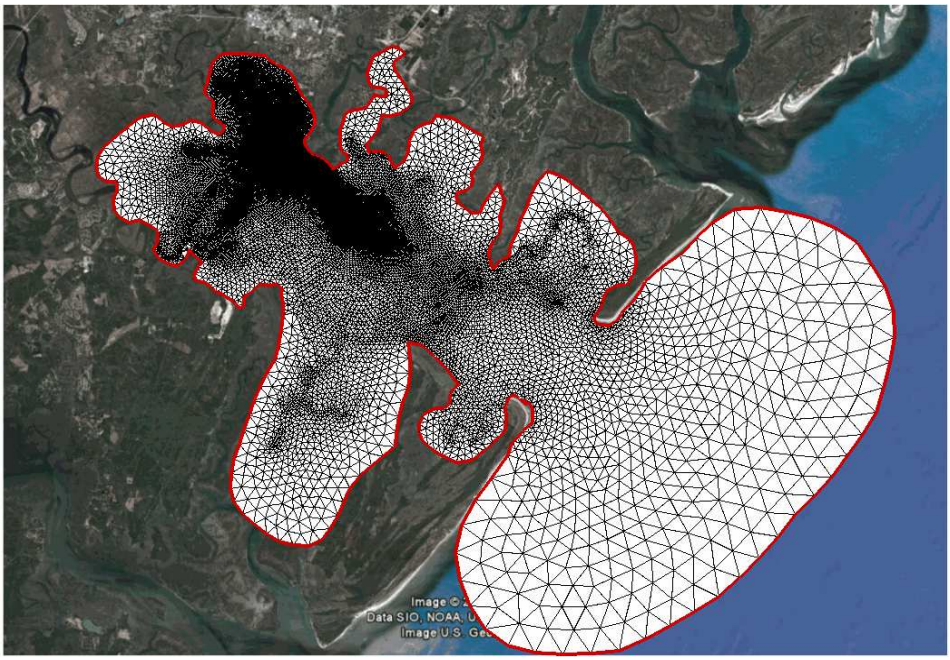

Figure 11*: Computational domain and numerical grid of the simulation*

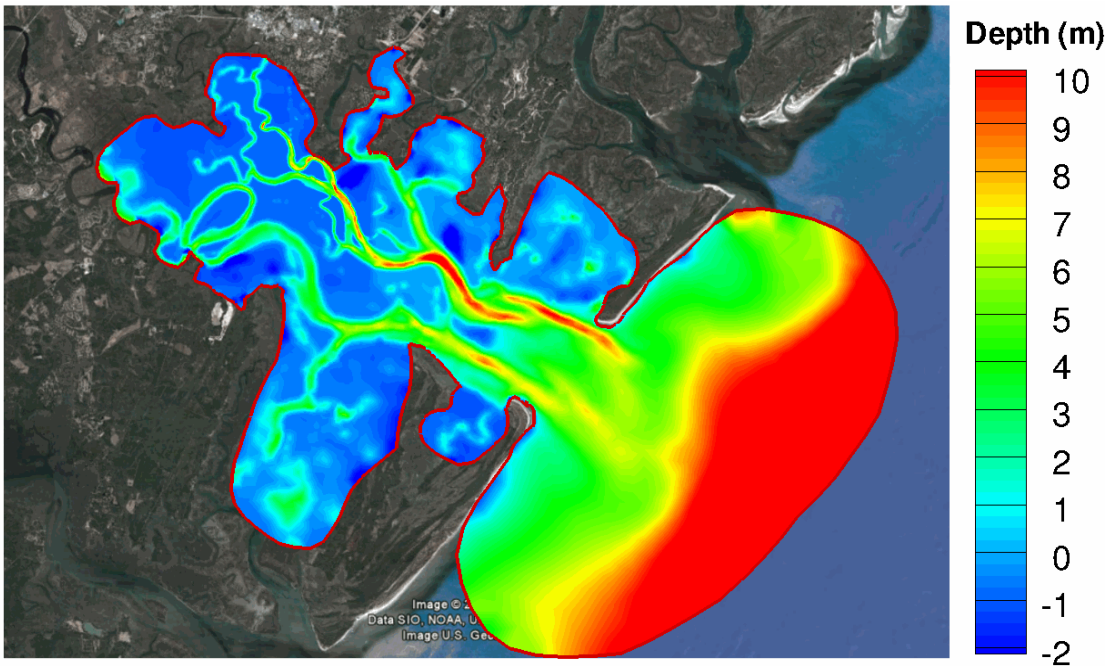

Figure 12*: Contours of the bathymetry in the computational domain*

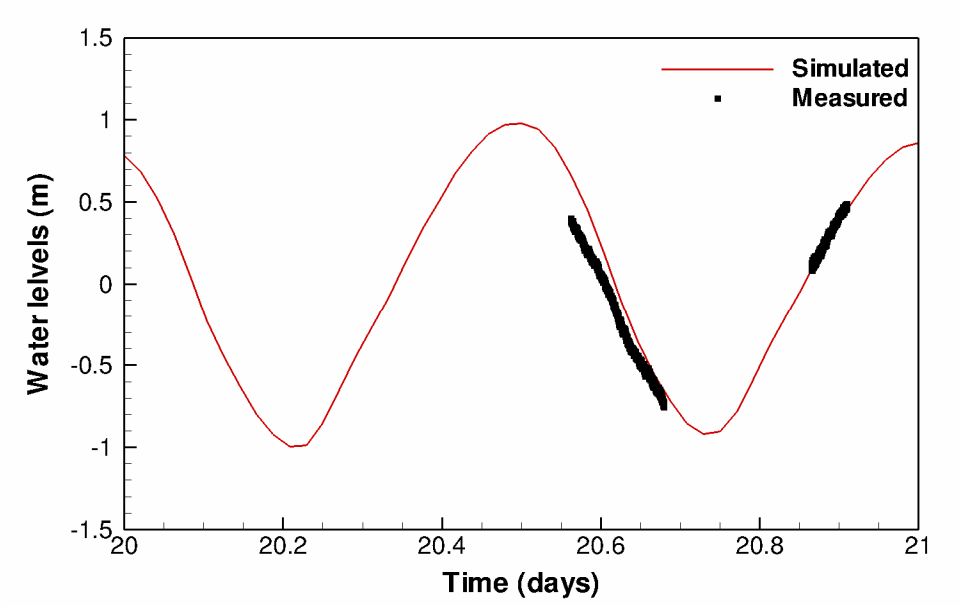

Figure 13*: Comparison of computed water levels represented as red line against field measurements represented by black symbols.*

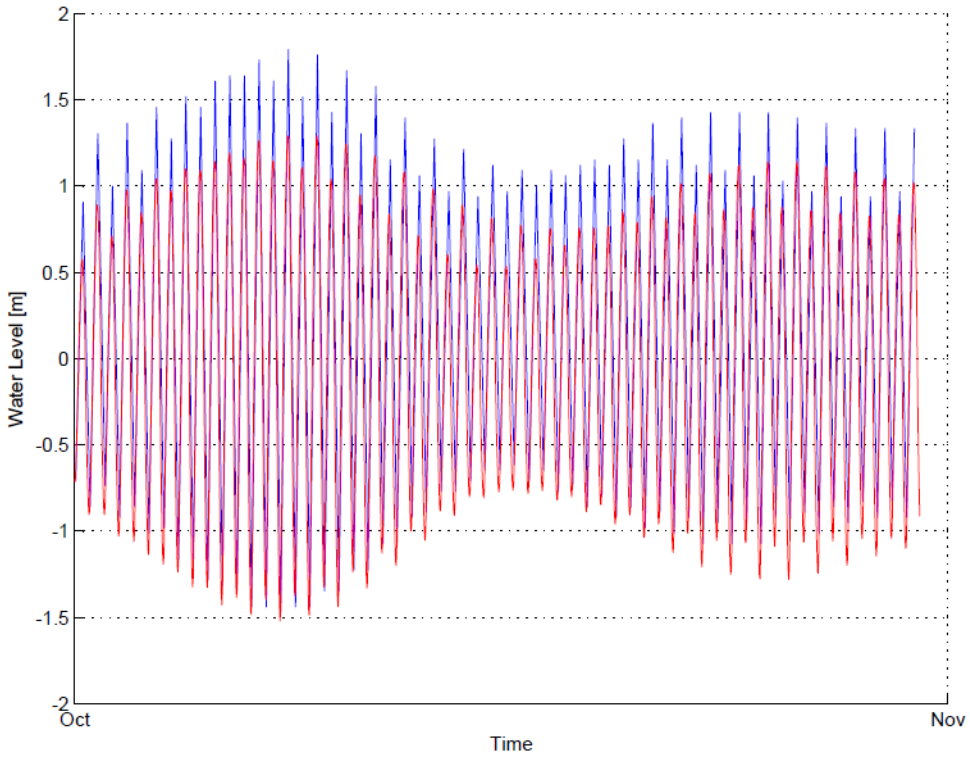

Figure 14*: Comparison of computed water levels represented as red line against observed measurements at Coffee Bluff Station of NOAA represented as blue line.*

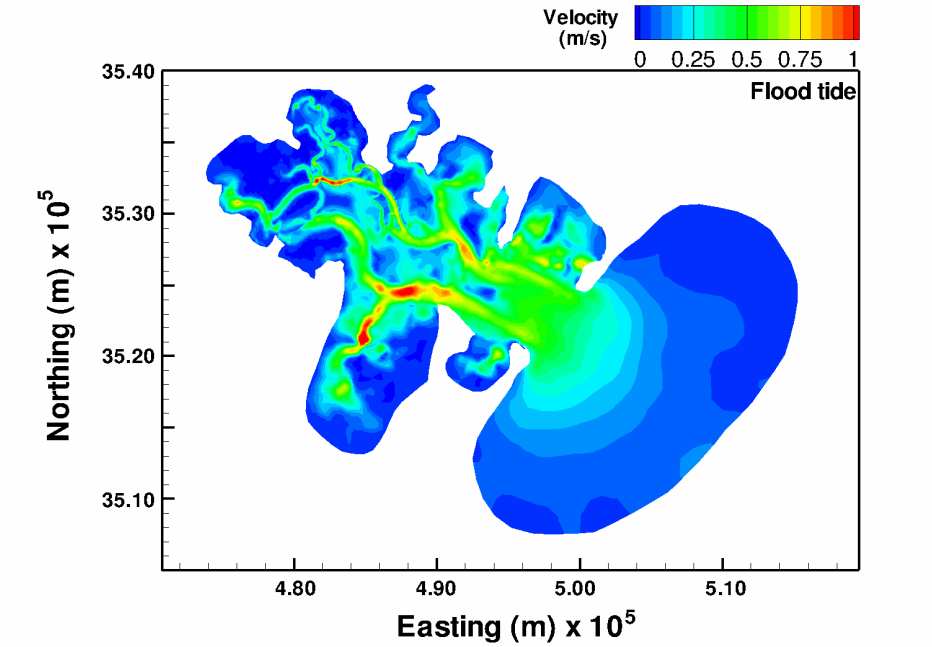

Figure 15*: Contours of the depth-averaged current magnitude in the entire Ogeechee estuary for a flood tide.*

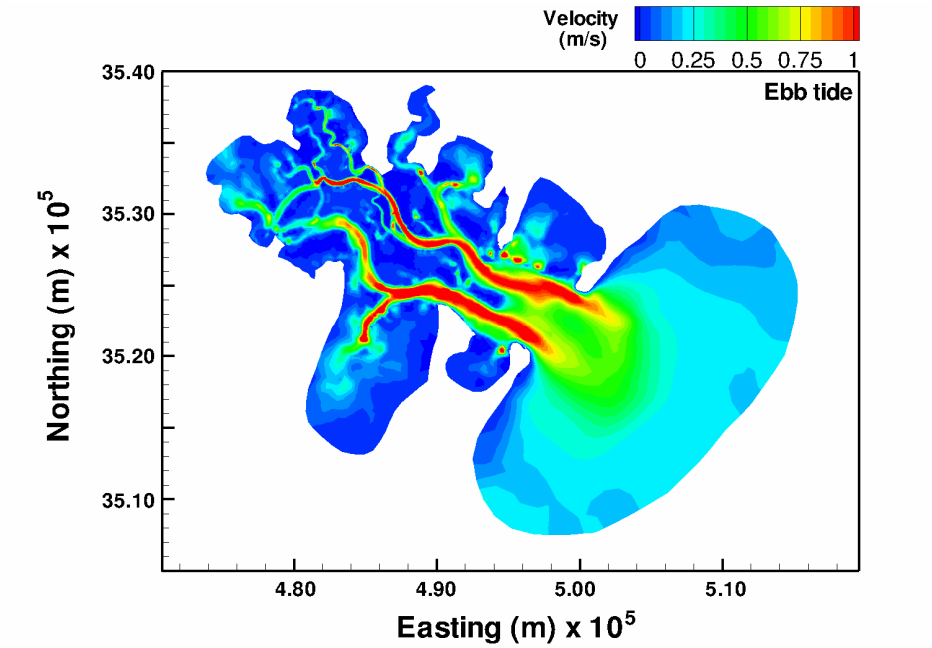

Figure 16*: Contours of the depth-averaged current magnitude in the entire Ogeechee estuary for an ebb tide.*

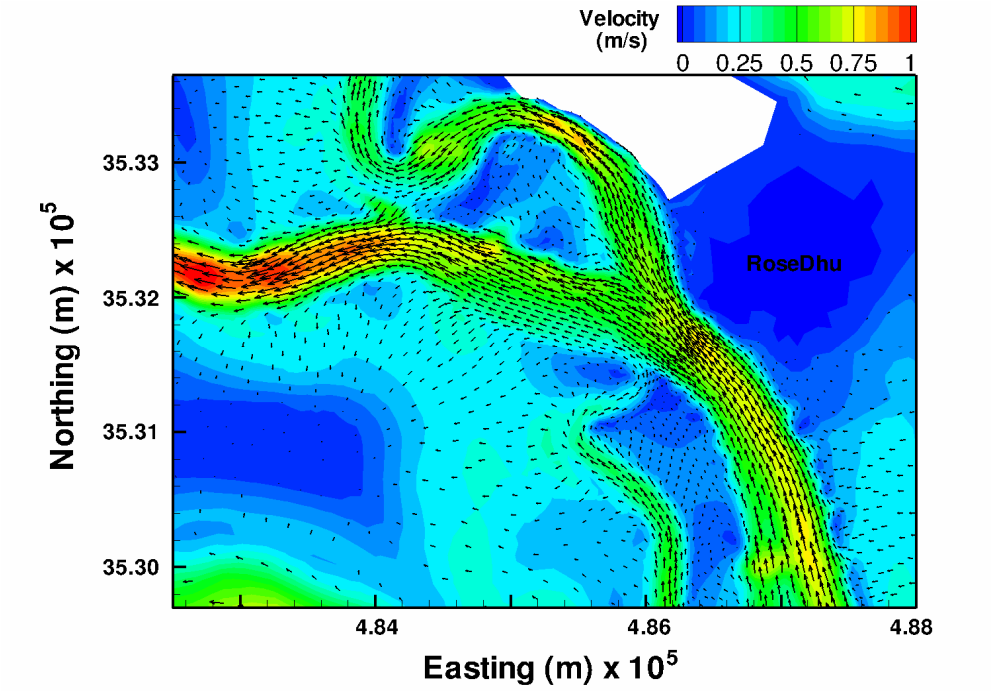

Figure 17*: Zoomed in contours of the depth-averaged current magnitude along with vectors at regions close to the Rose Dhu Island for a flood tide.*

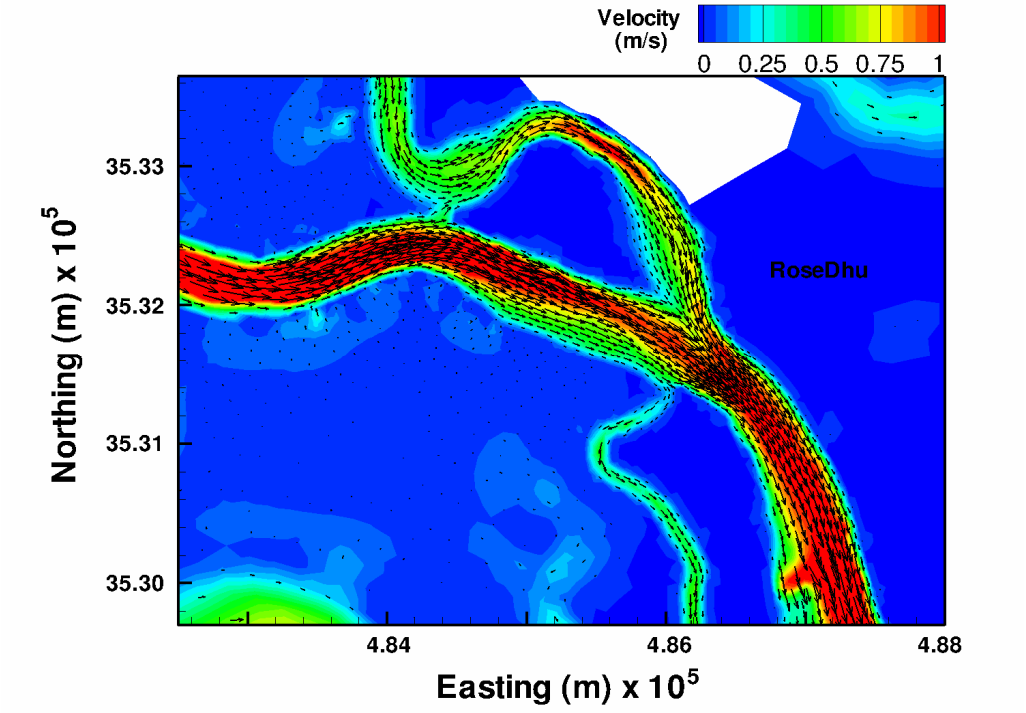

Figure 18*: Zoomed in contours of the depth-averaged current magnitude along with vectors at regions close to the Rose Dhu Island for an ebb tide.*

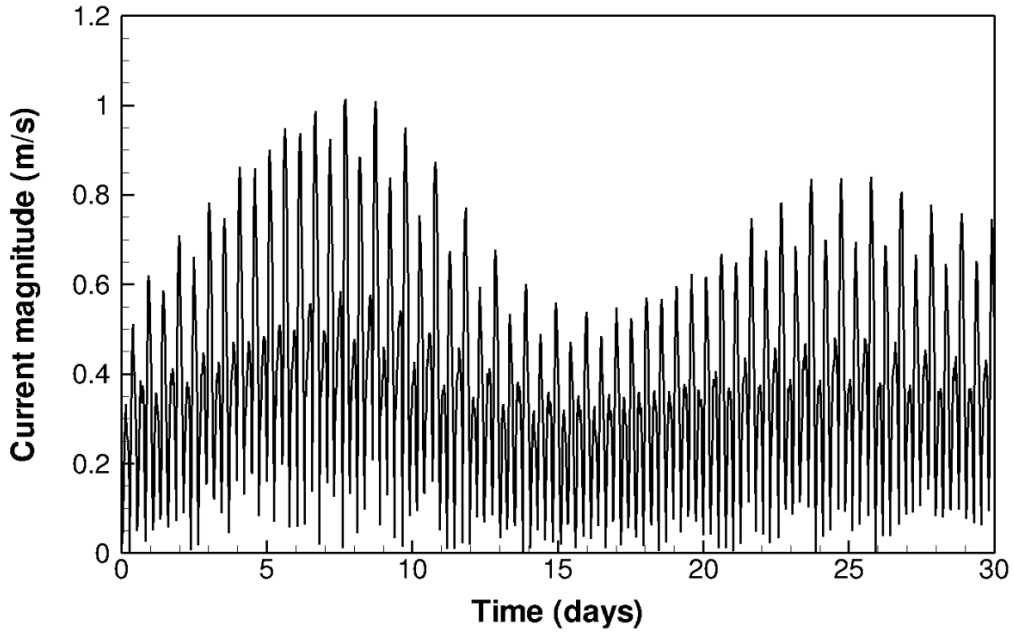

.

Figure 19*: One month time-series of the current magnitude at a selected location close to the Rose Dhu Island.*

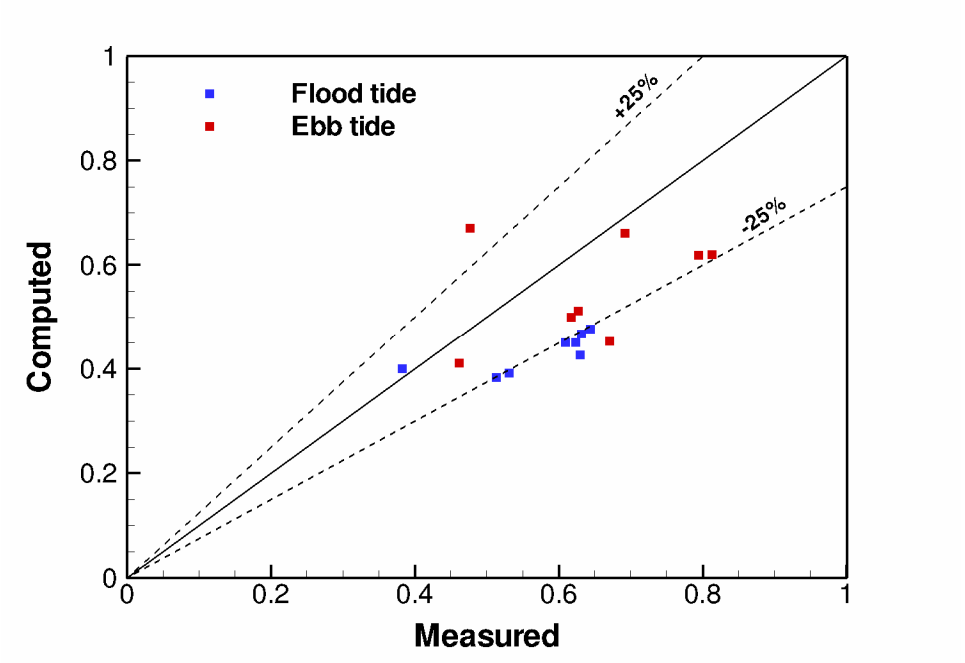

Figure 20*: Comparison of computed and measured depth-averaged current magnitudes for flood and ebb tides*

Objective 3: Accurate estimates of the maximum tidal stream power attainable via utilization of free-stream turbines.

1. **Problems encountered and unanticipated delays:** none

2. **Status:** completed.

Deliverables: Tidal energy assessment is conducted and an estimate of the total power that can be extracted is provided.

Power Calculations

Calculations are performed to determine the available theoretical kinetic power per unit area of vertical plane of water from the tidal streams surrounding Rose Dhu during a one year period. Three points in space are chosen for this analysis, all in close proximity to the 'hot spot' of high current velocities as seen in Figure 21. For each point, three time series, each a month long with a 30 minute time step starting from October 1, 2010 are extracted from the computational model; the time series consists of depth averaged current velocities in the East and North directions and water surface heights for each point.

In order to project future surface heights and velocities for an entire year, the tidal constituents for each are calculated via harmonic component analysis (Palowicz et al, 2002). Tidal constituents can reconstruct a water surface height signal by the series

$$\eta(t) = \sum_{i=1}^{I} [\![a_i \cos(\omega_i] + \phi_i)$$

where $\eta(t)$ is the water surface height for time t, i and I represent the i th constituent and total number of constituents respectively, and a_i, ω_i, and ϕ_i are the amplitude, angular frequency, and phase angle of the i th constituent respectively. Similarly, constituents for current velocities as well can be calculated through the use of complex amplitudes to resolve the directionality of the associated with the velocity. The resultant amplitudes, frequencies, and phase shifts for each constituent can be seen in Table 1.

The harmonic component analysis shows that tidal constituents, for all three points, can reconstruct over 98% of the total variance of the original signal for both current velocities and water surface heights. This overwhelming percentage is expected since no other forcing was introduced into the model. The dominant constituent for both current velocity and surface height is M2 (primary lunar semi-diurnal constituent with a period of 12.42 hours), which represents more than 89% of the total variance of each time series. Between points, amplitudes for each surface height constituent are found to

be relatively the same. Amplitudes of velocity constituents vary slightly between Points 1+2 which can be expected since current velocities have more spatial variability than surface heights due to the hydrodynamics of the channel. Velocity amplitudes of Point 3 are smaller as expected due to the branching of the main channel.

The derived constituents are used to forecast tidal stage and current velocity for an entire year with an hour time step for each point. In order to investigate the accuracy of these predictions, the forecasted water levels are compared with the field data obtained from all the surveys including the data from recent surveys in Nov and Dec 2011. This is shown in Figure 22 where validation plots of water levels are presented. Similarly current velocity magnitudes are calculated for each hour and are utilized to calculate a time series of the available kinetic power density by

$$p_{kinetic} = \frac{1}{2}\rho \left|\overrightarrow{V(t)}\right|^3$$

Where $\left|\overrightarrow{V(t)}\right|$ is the depth averaged current velocity magnitude for time t ,and ρ is the mass density of water assumed at 1025 kg m^{-3}. From such time series, histograms of the depth averaged velocity magnitudes and power density are produced for each point and are shown in Figure 23. The most occurring or most probable depth averaged velocity is between 0.5-0.6 m/s around the 'hot-spot' site. The most likely power density is shown to be the lowest bin with power densities under 20 W/m^2. This is a result of slack or diminishing ebb and flood tides dominating the 12- hour tidal cycle.

To provide a better indicator of available energy, the total power calculation is performed for points across an entire cross-section of transect 21, represented in Figure 21. In order to calculate the theoretical total power, a simplified method that considers both the kinetic and potential power with the exclusion of any technology specific assumptions is applied. The details of the method is outlined by Garrett and Cummins, 2005. The method uses the undisturbed flow field from the model with simple analytical methods, accounts for the cumulative effect of dissipating energy and provides information on an estuary scale.

Considering a constricted channel connecting two large bodies of water in which the tides at both ends are assumed to be unaffected by the currents through the channel, a general formula gives the maximum average power as between 20 and 24% of the peak tidal pressure head times the peak of the undisturbed mass flux through the channel. This maximum average power is independent of the location of the turbine fences along the channel. Maximum average tidal stream power, P_{max}, is given as

$$P_{max} = \gamma \cdot \rho \cdot g \cdot a \cdot Q_{max}$$

where γ is a parameter, ρ is the density of seawater, a is the amplitude of the tidal water level constituent and Q_{max} is the maximum corresponding tidal flow rate. For a background friction dominated, nonsinusoidal (i.e. considering more than one tidal constituent) case, if data for the head and flux in the natural state are available, the maximum average power may be estimated with an accuracy of 10% using γ = 0.22, without any need to understand the basic dynamical balance (Garrett and

Cummins, 2005). A multiplying factor is used to account for additional constituents (a_1, a_2, …) given as

$$1 + \left(\frac{9}{16}\right)(r_1^2 + r_2^2 + \cdots)$$

where $r_1 = \frac{a_1}{a}, r_2 = \frac{a_2}{a} \ldots$

This upper bound on the available power ignores losses associated with turbine operation and assumes that turbines are deployed in uniform fences, with all the water passing through the turbines at each fence. Using this method it was found that the total available power for transect 21 was 3.2MW.

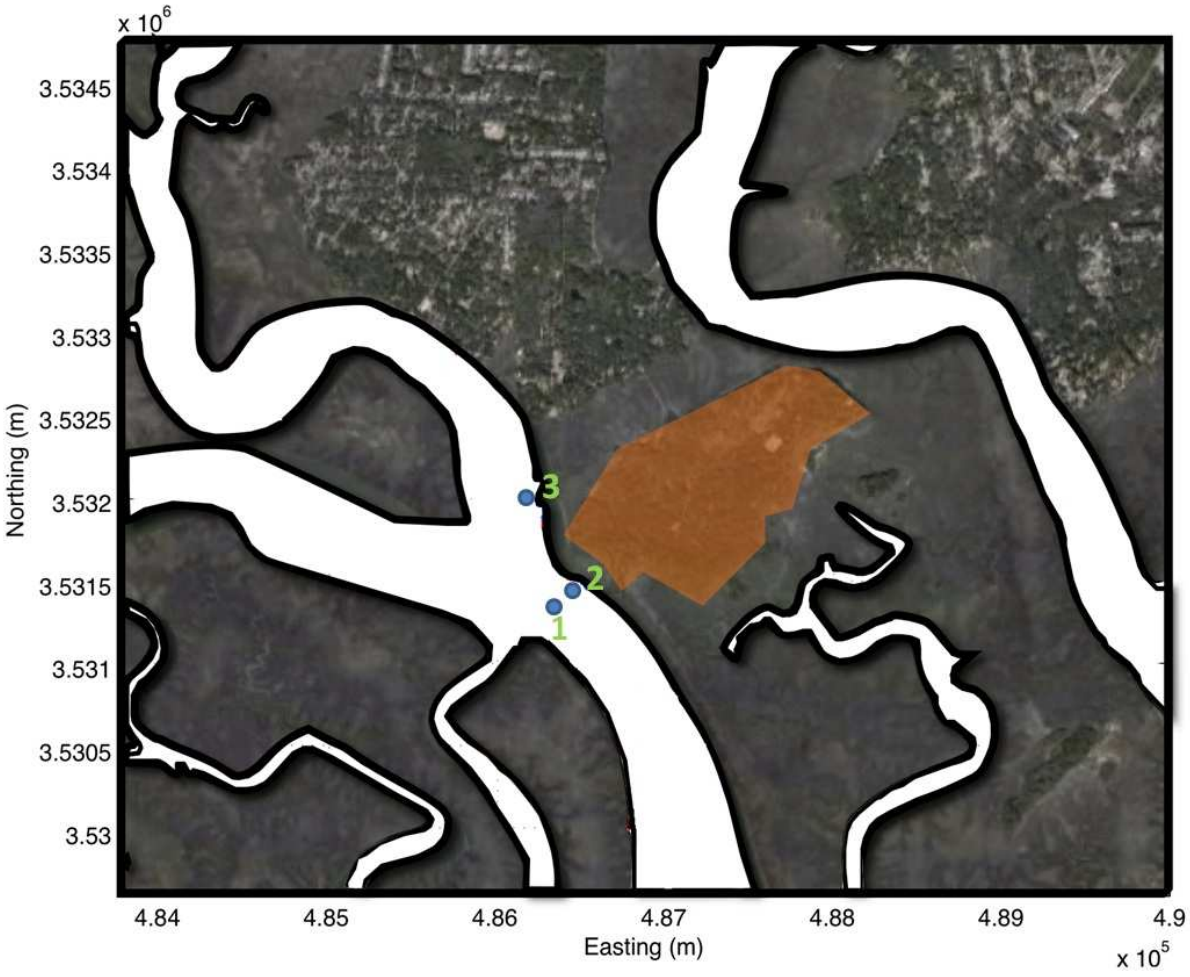

Figure 21*: Locations of three points selected for kinetic power density calculations and cross section selected for cumulative kinetic power calculation.*

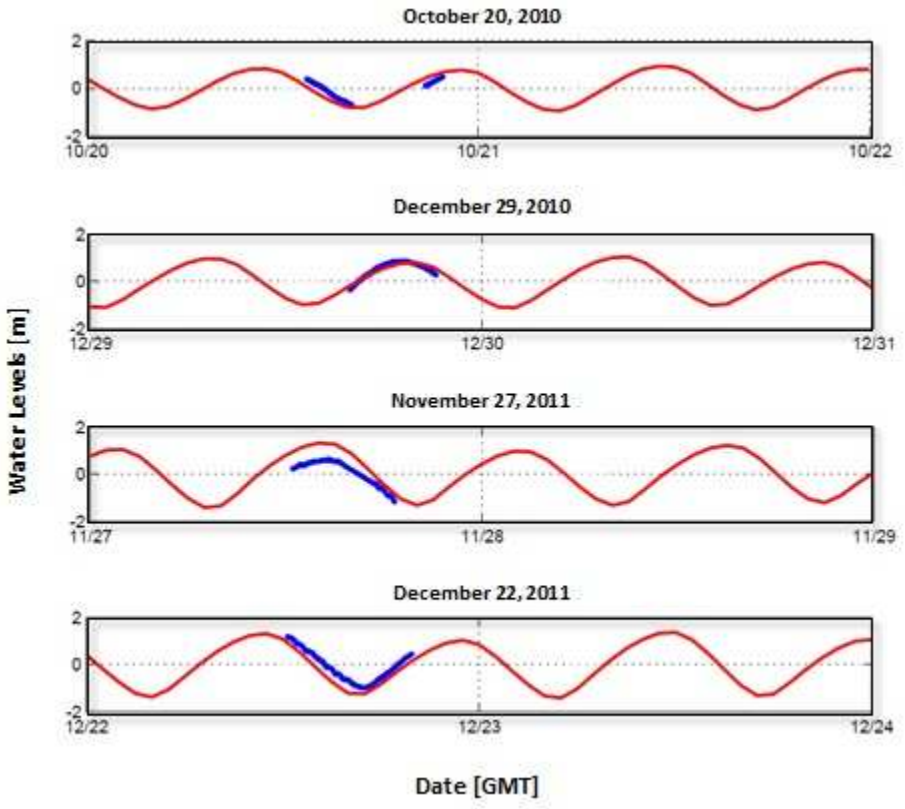

Figure 22*: Comparison of constructed water levels with the data from field surveys*

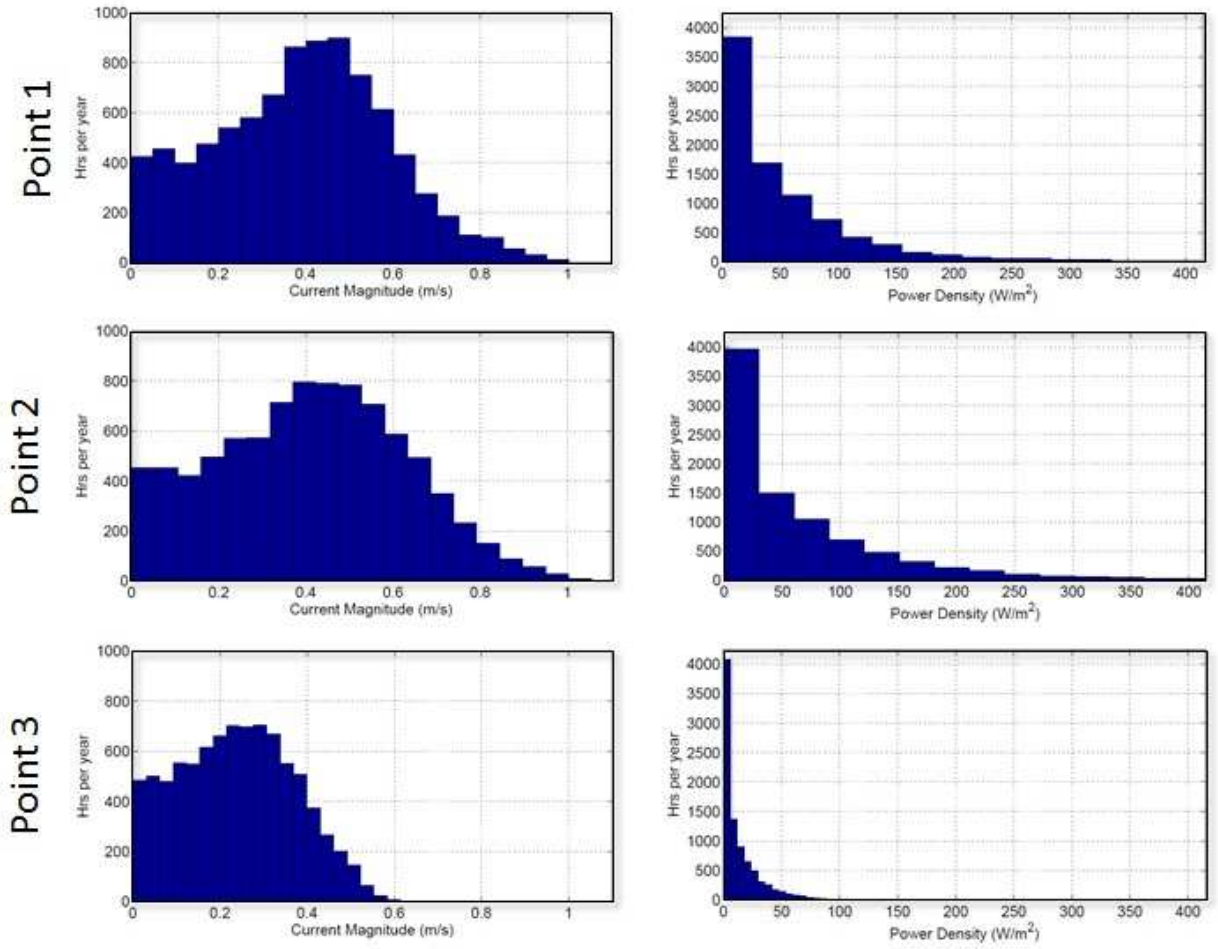

Figure 23*: Histograms of depth averaged current velocity magnitudes and power density at points 1, 2, and 3.*

Table 1 Harmonic analysis results derived from 31 day record of water surface heights and depth averaged current velocities for each selected point.

Period (Hrs)			
Constituent	**All Points**		
M2	12.42		
N2	12.66		
K1	23.93		
S2	12.00		
MN4	6.27		
O1	25.82		
MS4	6.10		
M4	6.21		
M6	4.14		
Water Surface Height Amplitude (m)			
Constituent	**Point 1**	**Point 2**	**Point 3**
M2	0.960	0.961	0.962
N2	0.197	0.197	0.197
K1	0.118	0.118	0.119
S2	0.182	0.182	0.182
MN4	0.035	0.035	0.037
O1	0.084	0.084	0.085
MS4	0.033	0.033	0.034
M4	0.080	0.080	0.083
M6	0.017	0.017	0.016
Current Velocity Amplitude (m/s)			
Constituent	**Point 1**	**Point 2**	**Point 3**
M2	0.582	0.615	0.354
N2	0.120	0.128	0.074
K1	0.048	0.052	0.035
S2	0.113	0.121	0.071
MN4	0.039	0.041	0.027
O1	0.035	0.039	0.027
MS4	0.036	0.037	0.024
M4	0.094	0.117	0.089
M6	0.043	0.040	0.027

Objective 4: Two technical interchange seminars will be held at Rose Dhu to disseminate project results and findings, and discuss emerging ideas with folks from SCAD, local universities, the Skidaway Institute of Oceanography, and local engineering companies.

1. **Problems encountered and unanticipated delays:** none

2. **Status:** partially completed.

3. **Deliverables**: A technical seminar has been held at Rose Dhu on August 20 (see attached agenda). The second seminar is planned in April-May 2012 at Tybee Island.

References

Chen, C., G. Cowles, and R.C. Beardsley. (2006). "An unstructured grid, finite volume coastal ocean model: FVCOM User Manual, Second Edition". SMAST/UMASSD Technical Report-06-0602.

Chen, C., Liu, H., and Beardsley, R.C. (2003). “An unstructured grid, fintie-volume, three-dimensional, primitive equation ocean model: application to coastal ocean and estuaries.” Journal of Atmospheric and Oceanic Technology, 20, 159-186.

Huang, H., Chen, C., Blanton, J.O., and Andrade, F.A. (2008). “A numerical study of tidal asymmetry in Okatee Creek, South Carolina.” Estuarine, Coastal and Shelf Science, 78, 190-202.

Mellor, G.L., and Yamada, T. (1982). “Development of a turbulence closure model for geophysical fluid problem.” Review of Geophysics and Space Physics, 20, 851-875.

Smagorinsky, J. (1963). “General circulation experiments with the primitive equations: I. The basic experiment.” Mon Weather Rev., 91, 99-164.